Frontiers in Bioscience Landmark

Front. Biosci. (Landmark Ed) **2026**; 31(5): 50425
https://doi.org/10.31083/FBL50425

Original Research

SIRT7 Prevents Intervertebral Disc Degeneration by Inhibiting the NF-κB Pathway

Dongxin Wang[1,2,3,4,†], Zhili Yang[1,2,3,4,†], Lei Li[1,2,3,4], Guangzhi Zhang[1,2,3,4], Zhenyu Cao[1,2,3,4], Tianyue Liu[1,2,3,4], Xuewen Kang[1,2,3,4,*]

[1]Department of Orthopedics, Lanzhou University Second Hospital, 730000 Lanzhou, Gansu, China
[2]The Second Clinical Medical College, Lanzhou University, 730000 Lanzhou, Gansu, China
[3]Key Laboratory of Orthopedics Disease of Gansu Province, Lanzhou University Second Hospital, 730030 Lanzhou, Gansu, China
[4]The International Cooperation Base of Gansu Province for The Pain Research in Spinal Disorders, 730030 Lanzhou, Gansu, China
*Correspondence: ery_kangxw@lzu.edu.cn (Xuewen Kang)
[†]These authors contributed equally.
Academic Editor: Elisa Belluzzi
Submitted: 26 January 2026 Revised: 10 March 2026 Accepted: 27 March 2026 Published: 26 May 2026

Abstract

Background: Nucleus pulposus (NP) cell apoptosis and extracellular matrix (ECM) degradation constitute the two major pathological hallmarks of intervertebral disc degeneration (IVDD). Inhibiting these deleterious processes represents an effective strategy for attenuating IVDD progression. Sirtuin 7 (SIRT7), a member of the sirtuin family, plays a critical role in modulating gene expression, mediating cellular stress adaptation, and facilitating DNA repair. While SIRT7 has demonstrated therapeutic potential across diverse pathological contexts, its specific contribution to IVDD pathogenesis remains elusive. This study aimed to delineate the functional contribution of SIRT7 to IVDD progression and unravel its molecular mechanisms. **Methods**:We quantified SIRT7 levels by immunohistochemistry (IHC) in degenerative human and rat NP tissues, and by quantitative reverse transcription polymerase chain reaction (qRT-PCR) in tert-butyl hydroperoxide (TBHP)-treated NP cells. To evaluate the protective capacity of SIRT7 overexpression, we conducted multifaceted analyses encompassing oxidative stress markers, apoptotic indices, ECM turnover, and nuclear factor kappa B (NF-κB) cascade activity in TBHP-challenged NP cells, utilizing reactive oxygen species detection probes, mitochondrial membrane potential indicators, Hoechst 33342 nuclear staining, qRT-PCR, western blotting, and immunofluorescence techniques. Its therapeutic potential was subsequently validated through magnetic resonance imaging and comprehensive histopathological evaluation (hematoxylin and eosin, Safranin O/Fast Green, and Masson trichrome staining) combined with IHC in a rat IVDD puncture model. **Results**: SIRT7 was consistently downregulated in degenerated human and rat NP tissues as well as TBHP-treated NP cells, concomitant with elevated NF-κB pathway activation. SIRT7 overexpression in TBHP-stimulated NP cells effectively attenuated oxidative stress, apoptosis, and ECM degradation. Mechanistically, SIRT7 overexpression may exert inhibitory effects on NF-κB signaling. Consistently, SIRT7 overexpression in the rat IVDD model decreased NF-κB activity, reduced NP cell apoptosis and ECM depletion, eventually ameliorating disc degeneration. **Conclusions**: Our findings demonstrate that SIRT7 expression declines progressively during IVDD development. SIRT7 overexpression protects against NP cell apoptosis and ECM degradation, and this protective effect correlates with inhibition of the NF-κB pathway. These findings suggest tha SIRT7 is a guardian of NP homeostasis and highlight its substantial promise as a molecular target for IVDD therapeutics.

Keywords: intervertebral disc degeneration; sirtuin7; NF-κB pathway; apoptosis; extracellular matrix

1. Introduction

Intervertebral disc degeneration (IVDD) is a slowly advancing pathological process involving progressive intervertebral disc (IVD) structural failure and functional impairment. This debilitating disorder culminates in chronic low back pain, imposing considerable socioeconomic burdens on healthcare systems worldwide [1]. Current management strategies, encompassing nonsteroidal anti-inflammatory agents and surgical procedures, provide merely symptomatic relief without halting disease advancement [2]. Therefore, the identification of safe and efficacious molecular targets holds substantial clinical and societal imperative.

Anatomically, the IVD comprises three distinct constituents: nucleus pulposus (NP), annulus fibrosus (AF), and cartilaginous endplates (CEP) [3]. The gelatinous NP serves as a critical shock-absorbing structure that facilitates uniform mechanical load distribution across the IVD, thereby safeguarding vertebral integrity. Through continuous synthesis of extracellular matrix (ECM) enriched in proteoglycans (predominantly aggrecan) and collagen II, NP cells preserve IVD functionality [4]. IVDD pathogenesis ensues when these resident cells succumb to apoptosis or alternative cell death modalities, accompanied by ECM degradation. Thus, diminished NP cell viability and ECM depletion represent the major pathological hallmarks of this disorder [3,5].

Copyright: © 2026 The Author(s). Published by IMR Press.
This is an open access article under the CC BY 4.0 license.

Publisher's Note: IMR Press stays neutral with regard to jurisdictional claims in published maps and institutional affiliations.

The nuclear factor kappa B (NF-κB) signaling pathway is a pivotal modulator in IVDD initiation and progression [6]. Previous investigations have demonstrated significant NF-κB pathway activation in human degenerative NP tissues and cells [7,8]. Multiple factors, including oxidative stress, mechanical load, and inflammatory cytokines, converge to activate NF-κB pathway, consequently regulating the expression of genes governing ECM degradation and apoptosis [9,10]. Therefore, pharmacological or genetic suppression of NF-κB activity represents a promising therapeutic strategy for IVDD intervention.

Sirtuin 7 (SIRT7) belongs to the evolutionarily conserved sirtuin protein family, functioning as a nicotinamide adenine dinucleotide (NAD^+) - dependent deacetylase [11, 12]. Despite its recent discovery, SIRT7 governs essential cellular functions including transcription, stress adaptation, and DNA repair, with promising implications for human disease treatment [13]. Yamamura *et al*. [14] have demonstrated that SIRT7-mediated deacetylation of GATA4 attenuates pathological cardiomyocyte hypertrophy. Additionally, SIRT7 fortifies cardiomyocyte resilience under pathological conditions, mitigating apoptosis and inflammation-mediated cardiac injury in murine models [15]. Yu *et al*. [16] established that SIRT7-mediated NRF2 activation via deacetylation enhances cellular antioxidant capacity and confers protection against chemotherapy-induced hepatic damage. Moreover, SIRT7 exerts protective effects against pulmonary hypertension through Krüpple-like factor 4 (KLF4) deacetylation and dampens inflammatory responses via NF-κB suppression [17,18]. Notably, downregulated SIRT7 expression has been documented in degenerative cartilage, where it serves as an essential guardian of cartilage homeostasis [19]. Nevertheless, SIRT7 expression patterns and its precise functional contribution to IVDD remain to be elucidated.

Accordingly, the present investigation sought to evaluate SIRT7 expression and explore its role in IVDD. We found that SIRT7 expression was markedly downregulated during IVDD progression. Functional rescue experiments revealed that SIRT7 overexpression could significantly inhibit NF-κB pathway activation, thereby effectively protecting NP cells from apoptosis and ECM breakdown *in vitro* and *in vivo*. Altogether, our findings suggest that SIRT7 acts as a previously unrecognized protector that maintains NP homeostasis and may be a potential therapeutic target for IVDD.

2. Materials and Methods

2.1 Human NP Tissues Collection

We obtained 12 NP tissue samples from patients who underwent surgery at the Department of Orthopedics, Lanzhou University Second Hospital, in 2025. During their lumbar IVD surgery, NP tissue was removed and transported to the laboratory. The samples were divided into the following two groups: a mild degeneration group (Grade II), which included NP tissues from three males and three females aged 22–46 years (mean age: 32.9 years), and a severe degeneration group (Grade V), which included NP tissues from three males and three females aged 47–69 years (mean age: 60 years). Exclusion criteria included history of spinal tumors, tuberculosis, or infectious diseases, consistent with previous studies [20].

2.2 Culture and Treatment of Rats NP Cells

For rat NP cell isolation, 4–6 weeks old Sprague–Dawley rats were deeply anesthetized via inhalation of 3–4% isoflurane until loss of pedal reflex, followed immediately by cervical dislocation as a secondary physical method to ensure definitive euthanasia [21], in accordance with the American Veterinary Medical Association (AVMA) Guidelines for the Euthanasia of Animals (2020). NP tissues were harvested from the IVD and digested with 0.5% type II collagenase (BS164; Biosharp, Hefei, Anhui, China) at 37 °C for 2 hours. The resulting cell suspension was cultured into DMEM/F-12 medium (C11330500BT, Gibco, Thermo Fisher Scientific, Suzhou, Jiangsu, China) supplemented with 10% FBS (FSP500, ExCell Bio, Suzhou, Jiangsu, China) and maintained in a humidified incubator at 37 °C with 5% CO_2 atmosphere. Upon reaching 80–90% confluency, cells were subcultured employing 0.25% trypsin–EDTA solution (T1300, Solarbio, Beijing, China). The cultured rat NP cells were validated for the NP cell–specific marker aggrecan by immunofluorescence staining (**Supplementary Material**) and tested negative for mycoplasma contamination. An oxidative stress environment was established *in vitro* by exposing the NP cells to the indicated concentrations of tert-butyl hydroperoxide (TBHP) (458139; Sigma-Aldrich, St. Louis, MO, USA) for 48 h. All *in vitro* experiments were independently performed three times.

2.3 Quantitative Reverse Transcription Polymerase Chain Reaction (qRT-PCR)

Total RNA was extracted with RNAiso Plus Reagent (9109, Takara Bio Inc., Kusatsu, Japan) and assessed for purity and concentration using NanoDrop 2000. After genomic DNA removal, the first-strand complementary DNA (cDNA) was synthesized using the Hifair® III 1st Strand cDNA Synthesis SuperMix for qPCR (gDNA digester plus) kit (H4509060, Yeasen Biotech, Shanghai, China). Quantitative polymerase chain reaction (PCR) proceeded on a QuantStudio 3 instrument (Thermo Fisher Scientific, Waltham, MA, USA) with Hieff® qPCR SYBR Green Master Mix (Low Rox Plus) kit (11202ES08, Yeasen Biotech, Shanghai, China) following the manufacturer's protocol. Relative expression was calculated by $2^{-\triangle\triangle Ct}$ method with β-actin as reference. Primers were synthesized by Tsingke Biotechnology (Beijing, China) (Table 1).

Table 1. The primers for qRT-PCR.

Gene	Forward primers 5′-3′	Reverse primers 5′-3′
SIRT7	TCCGTCAGGTGTCACGCATC	CCCTGAAGCTCGGTCACCA
Aggrecan	TGTCACTTCCCAACTATCCAGC	CCATGCATCACTTCACACCGAT
Collagen II	CCCCGGTCTTCCTGGTGTCA	CGCTCTCACCCTTCACACCT
MMP3	AACACTATGGAGCTGATGCAC	CTCAATGGCAGAATCCACAC
MMP13	CTACCATCCTGTGACTCTTGCG	TTTGCCAGTCACATCTAAGCC
Bax	GCCCCAGGACGCATCCACC	ACATGTCAGCTGCCACACGGAA
Bcl2	GGATGACTTCTCTCGTCGCTAC	ACACATGACCCCACCGAAC
β-actin	CATTGTCACCAACTGGGACGA	CATCTTTTCACGGTTGGCCTT

qRT-PCR, quantitative real-time polymerase chain reaction.

2.4 Western Blotting

NP cells were homogenized in ice-cold radioimmunoprecipitation assay (RIPA) buffer (P0013B, Beyotime, Shanghai, China) supplemented with protease inhibitor phenylmethylsulfonyl fluoride (PMSF) (ST506, Beyotime, Shanghai, China) and phosphatase inhibitors (P1091, Beyotime, Shanghai, China). Protein concentrations were spectrophotometrically measured via bicinchoninic acid (BCA) method (PC0020, Solarbio, Beijing, China). Equal amounts of protein were electrophoretically separated on polyacrylamide gels, transferred to polyvinylidene difluoride (PVDF) membranes (Millipore, Billerica, MA, USA), and blocked with 5 % skim milk or BSA. Membranes were subsequently probed with primary antibodies targeting SIRT7 (1:1000, 12994-1-AP, Proteintech, Wuhan, Hubei, China), matrix metalloproteinase-3 (MMP3) (1:4000, 66338-1-Ig, Proteintech, Wuhan, Hubei, China), phospho-p65 (p-p65, Ser536, 1:1000, 3033, CST, Danvers, MA, USA), total p65 (1:1000, 8242, CST, Danvers, MA, USA), or β-actin (1:5000, YM8343, Immunoway, Suzhou, Jiangsu, China) overnight at 4 °C, followed by HRP-conjugated goat anti-rabbit IgG (1:5000, GB23303, Servicebio, Wuhan, Hubei, China) or HRP-conjugated goat anti-mouse IgG (1:5000, GB23301, Servicebio, Wuhan, Hubei, China) incubation for 1 h. Bands were visualized with ECL (36208ES60, Yeasen, Shanghai, China) and imaged using a Chemiluminescence System (Surwit, Hangzhou, Zhejiang, China). Band intensities were quantified using ImageJ software (National Institutes of Health, Bethesda, MD, USA) and normalized to β-actin.

2.5 Intracellular Reactive Oxygen Species (ROS) Assay

Intracellular ROS accumulation was evaluated utilizing dihydroethidium (DHE) fluorescent probe (S0064S; Beyotime, Shanghai, China). Following loading with 10 μM DHE for 30 min, NP cells underwent triple PBS washes prior to immediate assessment of DHE-derived fluorescence via flow cytometric analysis (BD Biosciences, Franklin Lakes, NJ, USA) or inverted fluorescence microscopy (Zeiss, Jena, Thuringia, Germany).

2.6 Lentivirus Transfection

SIRT7-overexpressing lentiviruses (Lv-SIRT7) and a control lentivirus (Lv-NC) were purchased from GeneChem (Shanghai, China). At ~30% confluency, NP cells were transfected with Lv-SIRT7 (MOI = 50). Medium was changed after 48 h. SIRT7 overexpression was verified by qRT-PCR and Western blotting.

2.7 Measurement of Mitochondrial Membrane Potential ($\Delta\Psi m$)

$\Delta\Psi$m was measured using the MitoTracker Deep Red 633 fluorescent dye (C1997S, Beyotime, Shanghai, China). Briefly, NP cells were stained with 5 μM MitoTracker Deep Red 633 for 30 min at 37 °C in darkness, washed twice with PBS, and immediately analyzed using flow cytometry (BD Biosciences, Franklin Lakes, NJ, USA).

2.8 Hoechst 33342 Staining

After exposure to TBHP, NP cells were stained with 2 μM Hoechst 33342 (C1025, Beyotime, Shanghai, China) for 15 min at 37 °C in darkness. They were then rinsed thrice with PBS and observed under an inverted fluorescence microscope (Zeiss, Jena, Thuringia, Germany). Apoptosis was identified based on nuclear condensation, fragmentation, and intense blue fluorescence.

2.9 Immunofluorescence

NP cells plated in 24-well or confocal dishes underwent fixation with 4% paraformaldehyde for 20 min, followed by permeabilization using 0.5% Triton X-100 and blocking with 10% goat serum for 1 h. Overnight probing at 4 °C was conducted employing primary antibodies targeting aggrecan (1:200, DF7561, Affinity Bioscience, Changzhou, Jiangsu, China), collagen II (1:200, 28459-1-AP, Proteintech, Wuhan, Hubei, China), matrix metalloproteinase-13 (MMP13) (1:200, YT2796, Immunoway, Suzhou, Jiangsu, China), Bax (1:200, 60267-1-Ig, Proteintech, Wuhan, Hubei, China), Bcl-2 (1:200, 68103-1-Ig, Proteintech, Wuhan, Hubei, China), cleaved caspase-3 (1:200, 9664, CST, Danvers, MA, USA), or p65 (1:400, 8242, CST, Danvers, MA, USA). Subsequent to triple PBS rinses, specimens were exposed to cyanine

3- conjugated goat anti-rabbit IgG (1:200, GB21303, Servicebio, Wuhan, Hubei, China) or cyanine 3-conjugated goat anti-mouse IgG (1:200, GB21301, Servicebio, Wuhan, Hubei, China) for 1 h and nuclei were labeled with DAPI. Microscopic examination was carried out utilizing inverted fluorescence or confocal microscopy (Zeiss, Jena, Thuringia, Germany). For quantitative analysis, fluorescence intensity was measured using ImageJ software. Images were acquired under identical exposure settings across all groups. For NF-κB nuclear translocation assay, the nuclear-to-cytoplasmic fluorescence intensity ratio was calculated. For other immunofluorescence analyses, the integrated fluorescence intensity was normalized to the cell number to obtain mean fluorescence intensity. Images were captured from at least three randomly selected fields per sample, and experiments were repeated independently three times.

2.10 In Vivo Experiments

The rat model of IVDD was established according to a previously published protocol [22]. Twenty-eight 8-week-old male Sprague–Dawley rats (obtained from the Laboratory Animal Center of Lanzhou University) were randomly allocated into four groups: Sham, IVDD, IVDD + Lv-NC, and IVDD + Lv-SIRT7. The rats were sedated with 2% isoflurane (R510-22-10, RWD Life Science, Shenzhen, Guangdong, China) and subsequently anesthetized with 40 mg/kg intraperitoneal pentobarbital (SCRC 69020180, Sinopharm Chemical Reagent Shanghai Co., Ltd, China). Following sterile exposure of the Co7/8 disc, the NP was punctured with a 21G needle parallel to the CEP (360° rotation, 60 s), then injected with 3 µL of Lv-NC or Lv-SIRT7 (titer: 1×10^9 TU/mL) using a microliter syringe. The operator performing the surgeries was blinded to the group assignment. At the end of the experiment, the animals were euthanized using the method described in Section 2.2.

2.11 Magnetic Resonance Imaging (MRI)

MRI was conducted to evaluate the impact of SIRT7 on disc degeneration. At the eighth week post-operation, T2-weighted sagittal images were acquired using a uMR 9.4T small-animal MRI scanner (United Imaging Life Science Instrument, Wuhan, Hubei, China) via fast-spin echo (TR/TE = 3000/40 ms; matrix, 224 × 85; FOV, 17 × 45 mm; NEX, 4; and slice thickness, 0.5 mm contiguous).

2.12 Histological Analysis

Human NP and rat IVD samples were preserved in 4% paraformaldehyde, with rat samples additionally decalcified prior to processing. Following dehydration and paraffin embedding, 4 µm sections were stained with: hematoxylin and eosin (H&E) (G1120, Solarbio, Beijing, China) for general tissue architecture and cellularity; Safranin O/Fast Green (G1371, Solarbio, Beijing, China) and Alcian blue (G1560, Solarbio, Beijing, China) for matrix proteoglycans; Masson staining (G1346, Solarbio, Beijing, China) for collagen and fibrosis. Protocols followed manufacturer specifications, with Olympus microscopy used for imaging.

2.13 Immunohistochemistry (IHC) Staining

Paraffin sections of human NP and rat IVD samples underwent dewaxing, rehydration, and citrate-based antigen retrieval. Peroxidase quenching utilized 3% hydrogen peroxide (10 min) prior to overnight primary antibody binding at 4 °C: SIRT7 (1:200, DF6161, Affinity Bioscience, Changzhou, Jiangsu, China), aggrecan (1:100, DF7561, Affinity Bioscience, Changzhou, Jiangsu, China), collagen II (1:200, ab307674, Abcam, Cambridge, UK), MMP3 (1:200, ab52915, Abcam, Cambridge, UK), Bax (1:400, 60267-1-Ig, Proteintech, Wuhan, Hubei, China), or p65 (1:400, 8242, CST, Danvers, MA, USA). Immunoreactivity was visualized using an IHC detection kit (KIT-9710, Maixin Biotech Co., Fuzhou, Fujian, China) and DAB peroxidase substrate kit (KIT-0038, Maixin Biotech Co., Fuzhou, Fujian, China) per manufacturer instructions. For quantitative analysis, at least three fields within the NP region were randomly selected from each section, and positively stained cells (brown, DAB) and total cells (hematoxylin counterstain) were counted in each field. The percentage of positive cells was calculated as (positively stained cells / total cells) × 100%, and the mean value across all examined fields was used for statistical analysis.

2.14 Statistical Analysis

Quantitative results represent mean ± standard deviation (SD) from ≥3 independent trials. Statistical Analyses were performed using GraphPad Prism 9.0 (GraphPad Software, San Diego, CA, USA). Intergroup comparisons used two-tailed Student's *t*-test (two groups) or one-way analysis of variance (ANOVA) with Tukey's post-hoc test (multiple groups). Statistical significance was defined as $p < 0.05$.

3. Results

3.1 SIRT7 Expression Is Markedly Downregulated in Degenerative NP Tissues From Humans and Rats

SIRT7 expression and its association with IVDD were evaluated using human NP tissue of varying degenerative severity. Pfirrmann classification by T2-weighted MRI (Fig. 1A) was histologically confirmed through H&E, safranin O/fast green, and Alcian blue staining (Fig. 1B) and validated via IHC staining for aggrecan, collagen II, and MMP3 (Fig. 1C–F). IHC analysis revealed significantly lower SIRT7 levels in severe versus mild NP degeneration (Fig. 1C,G), indicating SIRT7 expression decline during disease progression.

These findings were verified in a puncture-induced rat IVDD model. Eight weeks post-surgery, MRI revealed reduced T2 signal intensity in punctured versus sham discs (Fig. 1H). Histological assessment via H&E, safranin O/fast

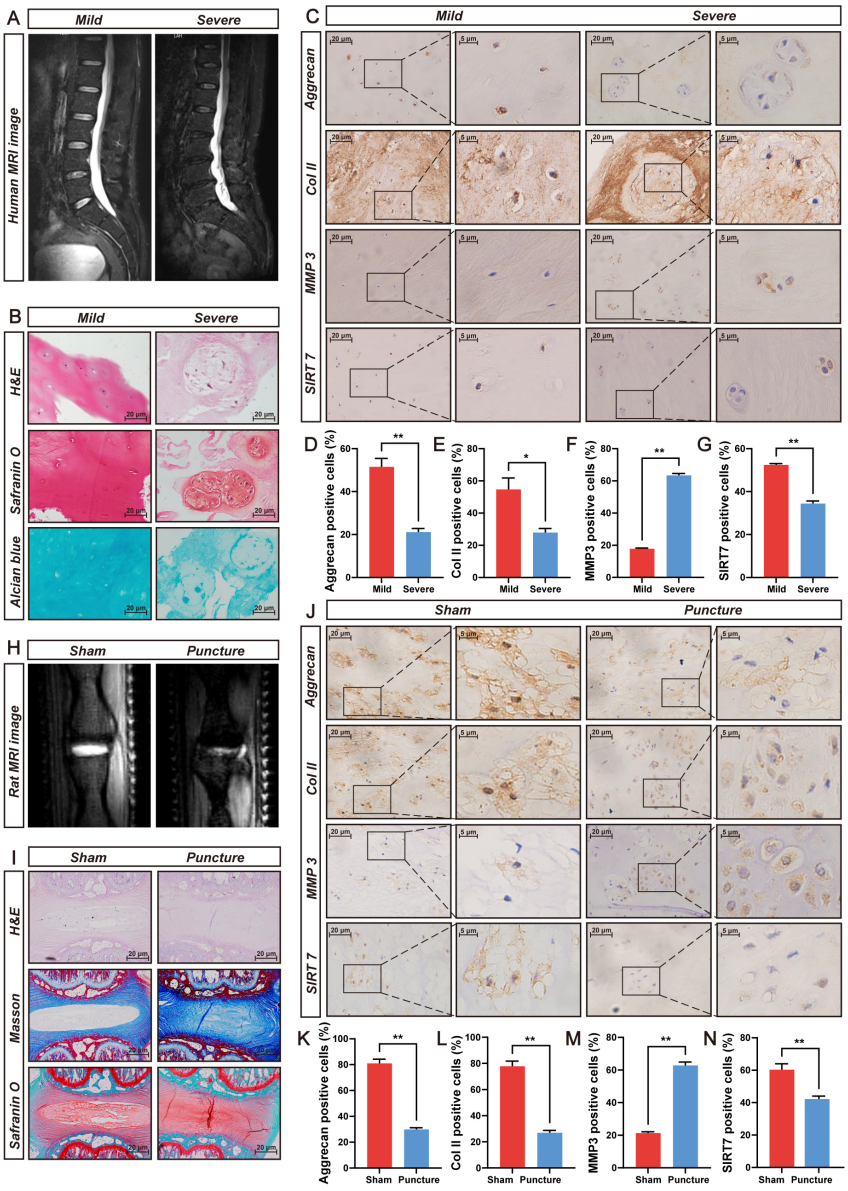

Fig. 1. SIRT7 expression is markedly downregulated in degenerated NP tissues from humans and rats. (A) Representative T2-weighted MRI scans illustrating mild (Pfirrmann Grade II) and severe (Pfirrmann Grade V) disc degeneration in patients. (B) Histological characterization of human NP specimens employing H&E, Safranin O/fast green, and Alcian blue staining. Scale bar: 20 μm. (C) IHC staining of aggrecan, Collagen II (Col II), MMP3, and SIRT7 in degenerative human NP tissue. Scale bar: 20 μm (main images) and 5 μm (insets). (D) Quantitative analysis of aggrecan immunoreactivity in degenerative human NP tissue. (E) Quantitative analysis of Col II immunoreactivity in degenerative human NP tissue. (F) Quantitative analysis of MMP3 immunoreactivity in degenerative human NP tissue. (G) Quantitative analysis of SIRT7 immunoreactivity in degenerative human NP tissue. (H) Typical T2-weighted MRI images captured from rats at 8 weeks post-needle puncture-induced IVDD surgery. (I) Histopathological evaluation of rat NP tissue utilizing H&E, Safranin O/fast green, and Masson's trichrome staining. Scale bar: 20 μm. (J) IHC detection of aggrecan, Col II, MMP3, and SIRT7 expression patterns in degenerated rat NP tissue sections. Scale bar: 20 μm (main images) and 5 μm (insets). (K) Quantitative analysis of positive staining rates for aggrecan in degenerative rat NP tissue. (L) Quantitative analysis of positive staining rates for Col II in degenerative rat NP tissue. (M) Quantitative analysis of positive staining rates for MMP3 in degenerative rat NP tissue. (N) Quantitative analysis of positive staining rates for SIRT7 in degenerative rat NP tissue. Quantitative results represent mean ± SD. Human samples: n = 6 (Grade II) and n = 6 (Grade V). Rat: n = 7 per group. The comparison between the two groups was conducted using Student's *t*-test. $*p < 0.05$, $**p < 0.01$. SIRT7, sirtuin 7; NP, nucleus pulposus; IHC, immunohistochemistry; H&E, hematoxylin and eosin; MMP3, matrix metalloproteinase-3; IVDD, intervertebral disc degeneration; SD, standard deviation; MRI, magnetic resonance imaging.

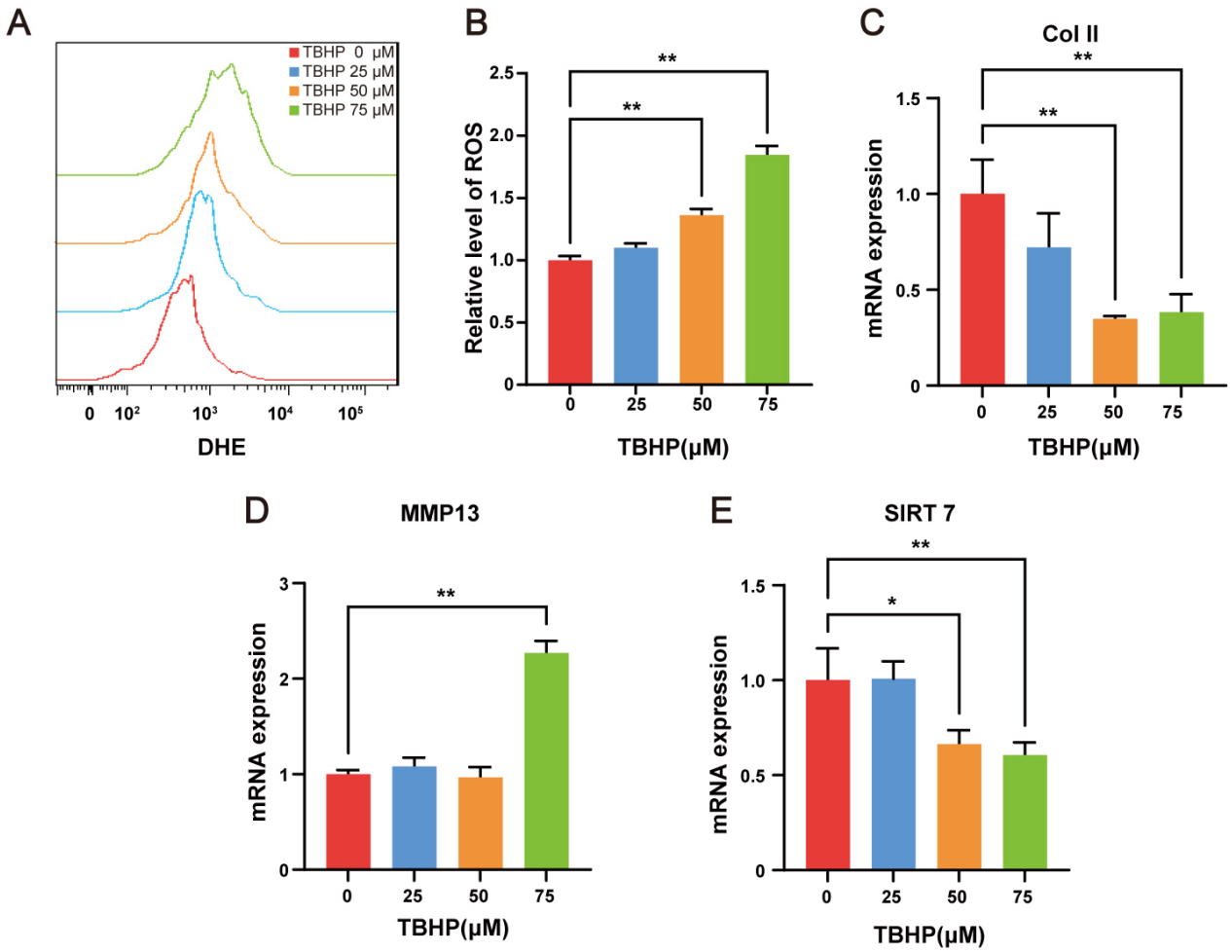

Fig. 2. SIRT7 is downregulated in TBHP-treated NP cells. (A) Flow cytometry histograms of DHE fluorescence after 48 h TBHP treatment. (B) Quantitative analysis of relative intracellular ROS levels, expressed as fold change in DHE mean fluorescence intensity relative to the control group. (C) qRT-PCR results for Col II in NP cells. (D) qRT-PCR results for MMP13 in NP cells. (E) qRT-PCR results for SIRT7 in NP cells. Values represent mean ± SD from three independent experiments. One-way ANOVA with Tukey's test. *$p < 0.05$, **$p < 0.01$. TBHP, tert-butyl hydroperoxide; DHE, dihydroethidium; ROS, reactive oxygen species; qRT-PCR, quantitative real-time polymerase chain reaction; ANOVA, analysis of variance.

green, and Masson staining revealed disrupted NP architecture, proteoglycan depletion, and fibrosis (Fig. 1I). Concurrent IHC analysis indicated decreased aggrecan, collagen II, and SIRT7 levels alongside elevated MMP3 (Fig. 1J–N). Together, these data suggest SIRT7 downregulation during IVDD.

3.2 SIRT7 Is Downregulated in TBHP-Treated NP Cells

ROS are considered a major pathological driving factor of IVDD. TBHP, an exogenous ROS donor, is widely used to establish cell models of IVDD *in vitro* [23]. To induce oxidative stress, NP cells were exposed to indicated concentrations of TBHP for 48 h. Intracellular ROS levels were subsequently quantified by flow cytometry following DHE labeling, revealing dose-dependent ROS accumulation (Fig. 2A,B). The qRT-PCR analysis demonstrated that 75 μM TBHP markedly suppressed collagen II expression (Fig. 2C) while upregulated MMP13 expression (Fig. 2D) in NP cells, thereby confirming the degenerative phenotype. Following validation of the cellular model, transcript level analysis revealed that SIRT7 expression was significantly downregulated in NP cells treated with 50 and 75 μM TBHP (Fig. 2E). These *in vitro* findings align with prior *in vivo* observations, collectively indicating decreased SIRT7 expression in NP cell degeneration. Accordingly, 75 μM TBHP was selected for subsequent experiments.

3.3 SIRT7 Overexpression Attenuates TBHP-Induced ECM Degradation in NP Cells

ECM homeostasis disruption underlies IVDD pathogenesis. To elucidate SIRT7's regulatory role in matrix metabolism, lentiviral-mediated SIRT7 overexpression was

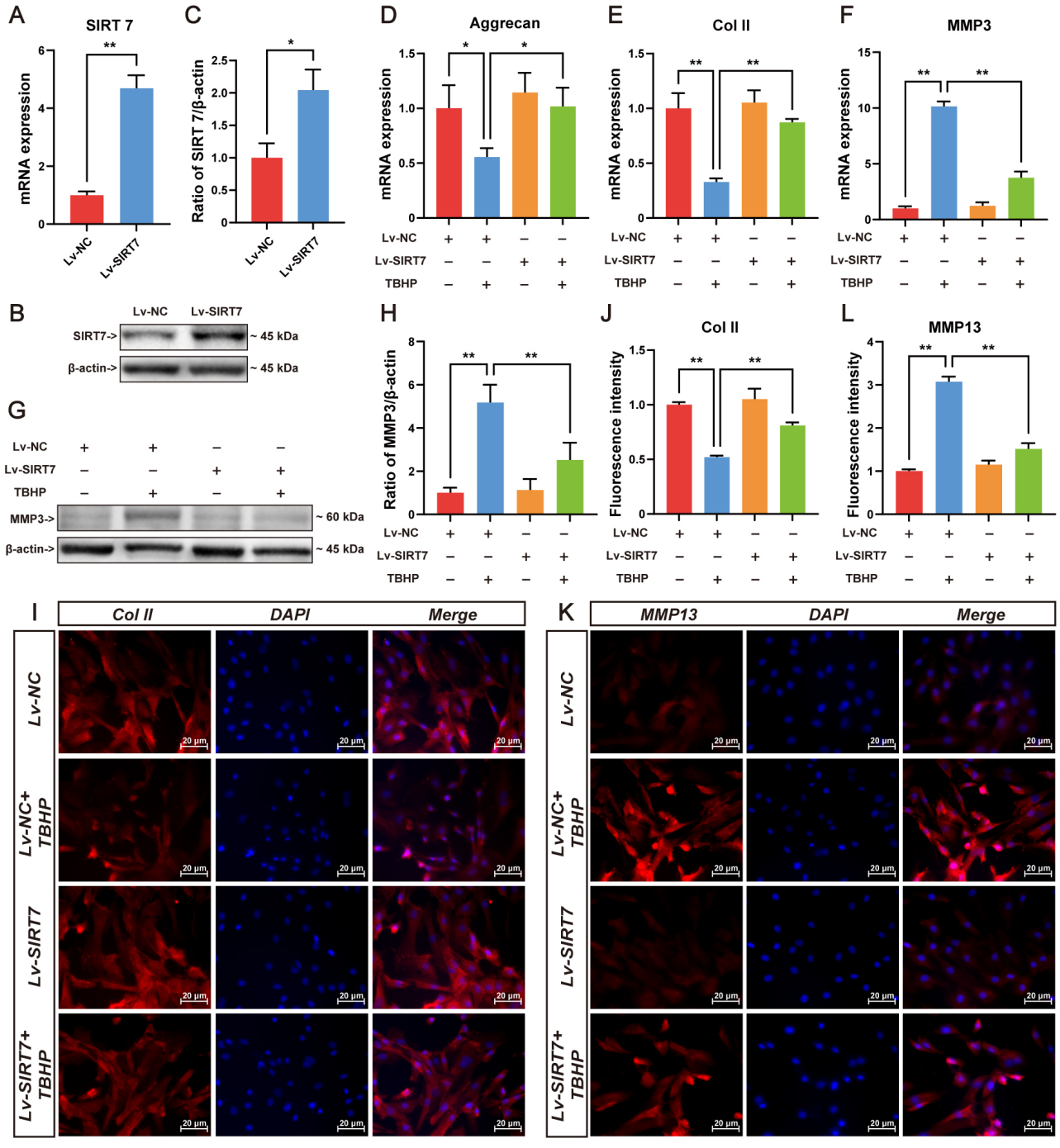

Fig. 3. SIRT7 overexpression attenuates TBHP-induced ECM degradation in NP cells. (A) SIRT7 transcript levels following lentiviral delivery evaluated by qRT-PCR. (B) Representative Western blot showing SIRT7 protein expression in transfected NP cells. (C) Quantification of SIRT7 protein levels normalized to loading control. (D) Aggrecan mRNA quantification by qRT-PCR. (E) Col II gene expression assessed through qRT-PCR. (F) MMP3 mRNA quantification by qRT-PCR. (G) Representative Western blot of MMP3. (H) Relative MMP3 protein quantification by Western blot. (I) Representative immunofluorescence staining images of Col II. Scale bar: 20 μm. (J) Quantitative immunofluorescence analysis of Col II in NP cells. (K) Representative immunofluorescence staining images of MMP13. Scale bar: 20 μm. (L) Quantitative immunofluorescence analysis of MMP13. Values represent mean ± SD from three independent experiments. Between-group differences analyzed by Student's *t*-test (two groups) or one-way ANOVA with Tukey's post-hoc test (multiple groups). $*p < 0.05$, $**p < 0.01$. –, untreated; +, treated. ECM, extracellular matrix; Lv-NC, control lentivirus; Lv-SIRT7, SIRT7-overexpressing lentivirus.

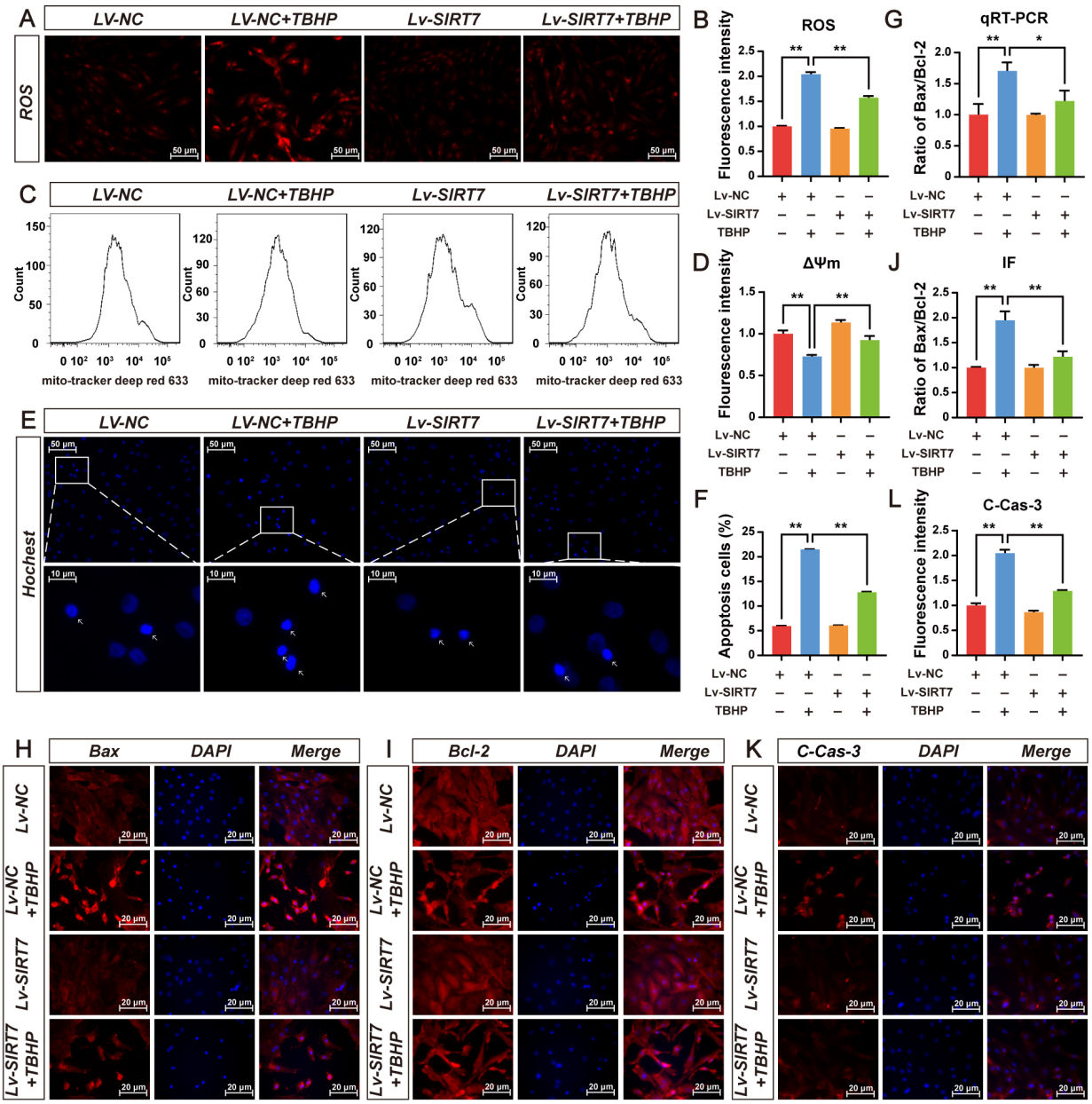

Fig. 4. SIRT7 overexpression protects NP cells from oxidative stress and apoptosis induced by TBHP. (A) Representative fluorescence micrographs of intracellular ROS detected by DHE staining in Lv-NC and Lv-SIRT7 groups treated with or without 75 μM TBHP for 48 h. Scale bar: 50 μm. (B) Quantitative assessment of intracellular ROS level in (A). (C) Representative flow cytometry histograms of ΔΨm detected with Mito-Tracker Deep Red 633. (D) Quantitative analysis of ΔΨm fluorescence intensities in (C). (E) Representative Hoechst 33342 staining images showing apoptotic morphology (white arrows). Scale bar: 50 μm (main images) and 10 μm (insets). (F) Apoptosis rate calculated from Hoechst 33342 staining. (G) qRT-PCR analysis of Bax/Bcl-2 ratio. (H) Representative immunofluorescence of Bax. Scale bar: 20 μm. (I) Representative immunofluorescence of Bcl-2. Scale bar: 20 μm. (J) Quantitative analysis of Bax/Bcl-2 ratio by immunofluorescence. (K) Representative immunofluorescence of C-Cas-3. Scale bar: 20 μm. (L) Quantitative analysis of C-Cas-3 by immunofluorescence. Values represent mean ± SD from three independent experiments. One-way ANOVA with Tukey's post-hoc test. *$p < 0.05$, **$p < 0.01$. –, untreated; +, treated. ΔΨm, mitochondrial membrane potential; C-Cas-3, cleaved caspase-3.

established in NP cells. The qRT-PCR (Fig. 3A) and Western blotting were performed to verify efficient SIRT7 upregulation in NP cells (Fig. 3B,C). Following oxidative challenge with TBHP, transcriptional profiling revealed substantial repression of aggrecan and collagen II alongside MMP3 induction, while SIRT7 overexpression reversed

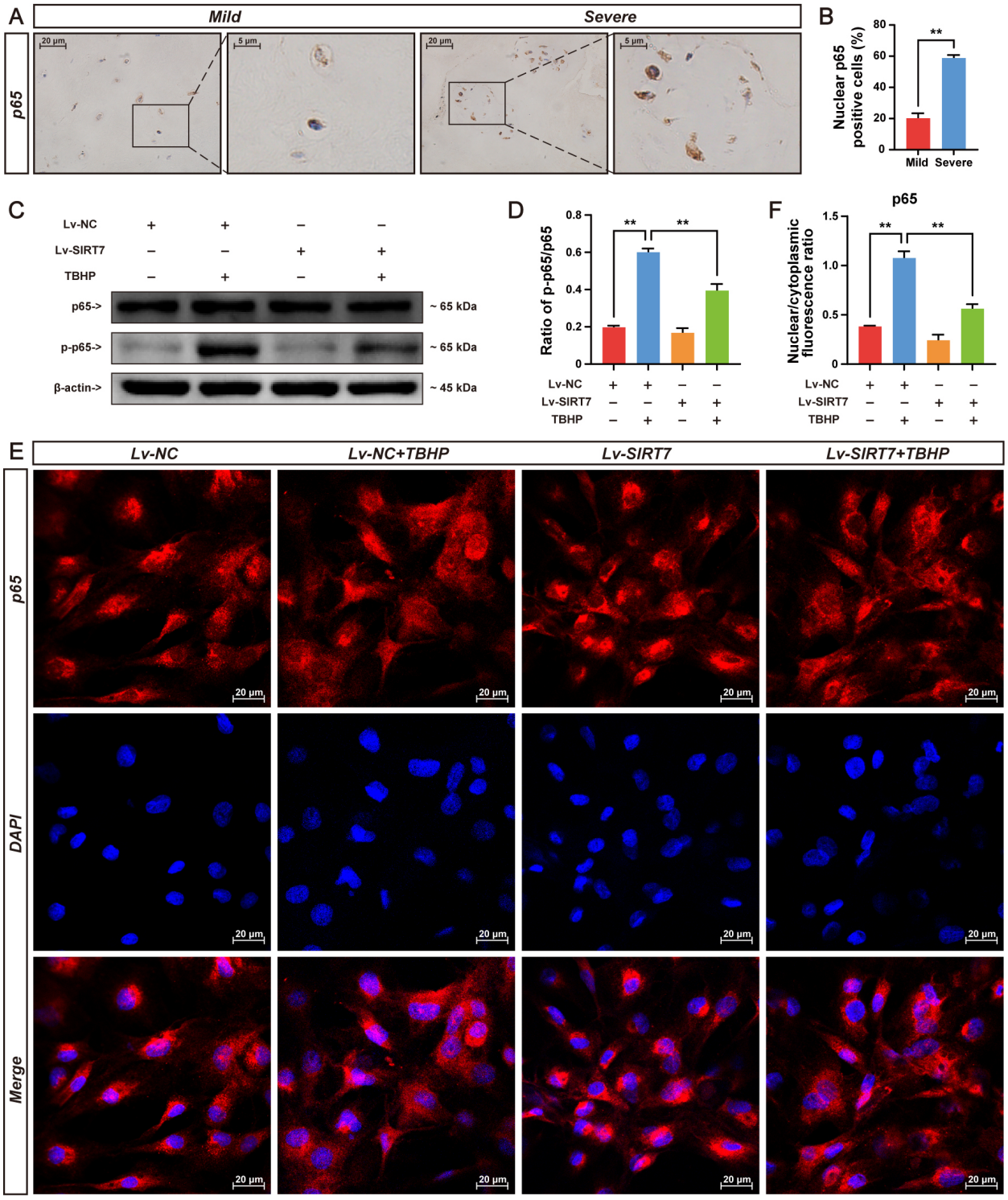

Fig. 5. SIRT7 overexpression inhibits NF-κB pathway activation in degenerative NP cells. (A) Representative IHC images demonstrating p65 distribution in human degenerative NP specimens. Scale bar: 20 μm (main images) and 5 μm (insets). (B) Semiquantitative assessment of nuclear p65 immunoreactivity. (C) Immunoblot detection of p-p65 and total p65 protein levels. (D) Densitometric quantification of p-p65 normalized to total p65. (E) Confocal immunofluorescence visualization of p65 subcellular compartmentalization. Scale bar: 20 μm. (F) Quantitative evaluation of p65 nuclear/cytoplasmic fluorescence intensity ratio. All data expressed as mean ± SD. Human samples: n = 6 (Grade II) and n = 6 (Grade V). Cell experiments: n = 3 independent experiments. Between-group differences analyzed by Student's *t*-test (two groups) or one-way ANOVA with Tukey's post-hoc test (multiple groups). $^{**}p < 0.01$. –, untreated; +, treated. NF-κB, nuclear factor kappa B; p-p65, phospho-p65 (Ser536).

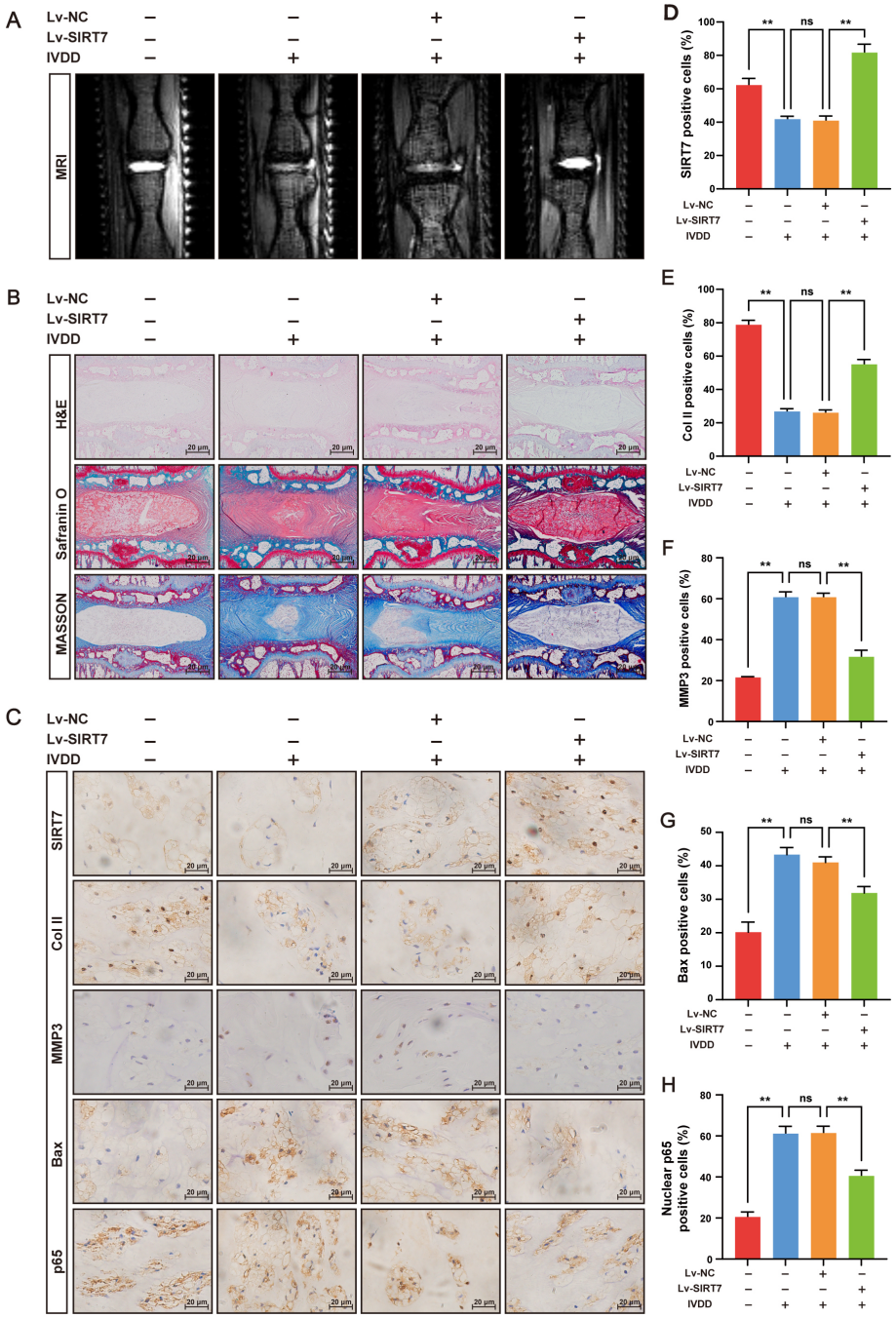

Fig. 6. SIRT7 overexpression alleviates IVDD in rats by suppressing the NF-κB pathway. (A) T2-weighted MRI acquired from experimental rats at eight weeks post-puncture. (B) Histological analysis of rat caudal disc specimens using H&E, Safranin O/fast green, and Masson staining. Scale bar: 20 µm. (C) Representative IHC images of SIRT7, Col II, MMP3, Bax, and p65. Scale bar: 20 µm. (D) Quantitative IHC analysis of SIRT7. (E) Quantitative IHC analysis of Col II. (F) Quantitative IHC analysis of MMP3. (G) Quantitative IHC analysis of Bax. (H) Quantitative IHC analysis of nuclear p65 protein expression. Values represent mean ± SD. Rat: n = 7 per group. Group comparisons employed one-way ANOVA followed by Tukey's post-hoc test. $^{**}p < 0.01$. ns, not significant. –, untreated; +, treated.

these TBHP-induced alterations (Fig. 3D–F). At the protein level, SIRT7 attenuated MMP3 accumulation (Fig. 3G,H), enhanced collagen II deposition (Fig. 3I,J), and diminished MMP13 immunoreactivity (Fig. 3K,L). Collectively, these findings suggest that SIRT7 upregulation preserves matrix integrity under oxidative stress, thereby retarding degenerative progression.

3.4 SIRT7 Overexpression Protects NP Cells From Oxidative Stress and Apoptosis Induced by TBHP

DHE staining showed that TBHP significantly increased intracellular ROS levels, whereas SIRT7 overexpression effectively inhibited TBHP-induced increase in ROS (Fig. 4A,B). Increased ROS triggers a decrease in $\Delta\Psi m$, which suggests an early apoptotic event. $\Delta\Psi m$ was measured using Mito-Tracker Deep Red 633, and flow cytometry revealed that TBHP depolarized $\Delta\Psi m$, but SIRT7 overexpression significantly inhibited this effect (Fig. 4C,D). Apoptotic morphology characterized by nuclear condensation, fragmentation, and intense blue fluorescence was observed by Hoechst 33342 staining. The results showed that TBHP promoted NP cell apoptosis, while SIRT7 overexpression markedly inhibited this effect (Fig. 4E,F). qRT-PCR and immunofluorescence analyses of the anti-apoptotic protein Bcl-2 and the pro-apoptotic protein Bax indicated that TBHP increased the Bax/Bcl-2 ratio, whereas SIRT7 overexpression significantly decreased this ratio (Fig. 4G–J). Similarly, immunofluorescence analysis of cleaved caspase-3 showed that TBHP increased cleaved caspase-3 levels, whereas SIRT7 overexpression markedly decreased these levels (Fig. 4K,L). Altogether, these data demonstrate that SIRT7 overexpression attenuates TBHP-induced oxidative stress and apoptosis in degenerative NP cells.

3.5 SIRT7 Overexpression Inhibits NF-κB Pathway Activation in Degenerated NP Cells

Accumulating evidence has established NF-κB as a well-characterized driver of apoptosis and ECM degradation in IVDD. Accordingly, targeted suppression of the NF-κB pathway effectively attenuates these pathological processes [23,24]. To explore whether SIRT7-mediated protection against apoptosis and matrix breakdown involves NF-κB pathway modulation, we evaluated NF-κB activation in TBHP-treated NP cells. p65 serves as a crucial component of the NF-κB pathway, wherein its phosphorylation status and nuclear translocation from the cytoplasm are critical indicators for evaluating NF-κB pathway activation state [9]. IHC staining of human specimens revealed higher nuclear p65 protein expression in severely degenerated discs than in mildly degenerated ones (Fig. 5A,B), confirming that NF-κB activation correlates with IVDD severity. Subsequently, we performed Western blotting and immunofluorescence assays to investigate whether SIRT7 overexpression could inhibit NF-κB activation induced by TBHP in NP cells. Western blotting showed that, compared with the control, TBHP had no effect on total p65 expression, but significantly increased phosphorylated p65 (p-p65) expression and the p-p65/p65 ratio, whereas SIRT7 overexpression inhibited these effects (Fig. 5C,D). Consistent with the results of Western blotting, immunofluorescence analysis revealed that TBHP induced p65 nuclear translocation, whereas SIRT7 overexpression attenuated it (Fig. 5E,F). Altogether, these results suggest that SIRT7 overexpression suppresses the NF-κB pathway activation in TBHP-induced NP cells.

3.6 SIRT7 Overexpression Alleviates IVDD in Rats by Suppressing the NF-κB Pathway

We established an IVDD rat model via needle puncture to evaluate the therapeutic potential of SIRT7 *in vivo*. Twenty-eight Sprague–Dawley rats were randomly assigned to sham, IVDD, IVDD + Lv-NC, or IVDD + Lv-SIRT7 groups. With the exception of sham-operated animals, rats in the other groups were injected with PBS, Lv-NC, or Lv-SIRT7, respectively. Eight weeks later, T2-weighted MRI was performed, and the IVD was harvested for histological and IHC analyses. As shown in Fig. 6, SIRT7 overexpression significantly attenuated IVDD progression. IHC analysis revealed that SIRT7 expression was markedly upregulated in the NP tissue of the IVDD + Lv-SIRT7 group compared with that in the other groups (Fig. 6C,D), confirming the successful overexpression of SIRT7. MRI showed that the T2-weighted signal intensity was considerably preserved in the IVDD + Lv-SIRT7 group compared with that in the IVDD and IVDD + Lv-NC groups (Fig. 6A). Consistent with this, histological analysis by H&E, Safranin O/fast green, and Masson staining revealed severe NP collapse, proteoglycan loss, and fibrosis in the IVDD and IVDD + Lv-NC groups; however, these degenerative changes were significantly attenuated in the IVDD+Lv-SIRT7 group (Fig. 6B). Additionally, IHC for collagen II, MMP3, and Bax showed that collagen II expression was downregulated, whereas MMP3 and Bax expression were upregulated in the IVDD and IVDD + Lv-NC groups, indicating increased ECM degradation and NP cell apoptosis. SIRT7 overexpression reversed these pathological changes (Fig. 6C,E–G). Importantly, nuclear p65 protein levels were significantly lower in the IVDD + Lv-SIRT7 group than in the IVDD and IVDD + Lv-NC groups (Fig. 6C,H), indicating that SIRT7 inhibits NF-κB activation. These data suggest that SIRT7 overexpression mitigates IVDD progression *in vivo*, and its protective effect may be associated with NF-κB inhibition.

4. Discussion

To the best of our knowledge, this study represents the first attempt to characterize SIRT7 expression patterns in IVDD and to investigate its cytoprotective potential in NP cells. Our data revealed a significant reduction in SIRT7 expression within human degenerative NP specimens. Comparable outcomes were observed in both the needle-puncture-induced rat IVDD model and TBHP-induced NP cell degeneration model. Functional experiments showed that SIRT7 overexpression protected NP cells from apoptosis and ECM breakdown, and this protective effect correlated with NF-κB signaling pathway inhibition *in vitro* and *in vivo*. Taken together, these findings

underscore that SIRT7 functions as an essential guardian of NP homeostasis and constitutes a compelling therapeutic target for IVDD management.

IVDD constitutes the predominant pathological basis of chronic low back pain. Despite incomplete mechanistic understanding, NP cell apoptosis and ECM deterioration represent hallmark pathological processes in this disease. Thus, suppression of cell apoptosis and restoration of matrix homeostasis constitute fundamental therapeutic strategies for this disease [25,26]. Oxidative stress, driven primarily by ROS overproduction, critically impairs NP cell function [27]. Oxidative stress not only induces NP cell apoptosis but also compromises ECM integrity, thereby accelerating IVDD. TBHP is an exogenous oxidant and extensively employed for *in vitro* degeneration modeling [23]. It rapidly elevates intracellular ROS levels and recapitulates apoptotic and catabolic phenotypes observed in human pathological specimens. Based on our observation that SIRT7 expression was decreased in degenerative NP tissues from both humans and rats, as well as in TBHP-stimulated NP cells, we conducted functional rescue experiments to evaluate the potential protective effects of SIRT7 overexpression against TBHP-induced injury. We found that TBHP challenge induced robust ROS generation, $\Delta\Psi$m dissipation, cell morphological changes, increased Bax/Bcl-2 ratio and elevated cleaved caspase-3 levels. Notably, SIRT7 overexpression significantly reversed these changes, demonstrating its protective capacity against oxidative stress and NP cell apoptosis triggered by TBHP. Furthermore, SIRT7 overexpression effectively restored ECM metabolic homeostasis disrupted by TBHP treatment, as evidenced by upregulated aggrecan and collagen II expression alongside downregulated MMP3 and MMP13 expression. Collectively, these results indicate that SIRT7 overexpression protects NP cells from oxidative stress, apoptosis, and ECM degradation induced by TBHP, thereby attenuating IVDD progression.

NF-κB serves as a pivotal regulator of NP cell apoptosis and ECM breakdown in IVDD pathogenesis. Under basal conditions, this transcription factor is retained in the cytoplasm in a quiescent state via tethering to IκB inhibitory molecules. Following oxidative insult, IκB proteins become phosphorylated and are targeted for proteasome-mediated destruction, enabling the unleashed NF-κB p65 subunit to translocate into the nucleus and drive the expression of downstream genes involved in ECM breakdown and apoptotic signaling [6]. Therefore, pharmacological or genetic inhibition of NF-κB pathway activation has emerged as a promising therapeutic avenue for IVDD intervention [23]. In the present study, we first confirmed that NF-κB activation was markedly elevated in severely degenerated human NP tissue compared with mildly degenerated specimens. To further investigate whether suppression of NF-κB signaling underlies the protection of SIRT7 overexpression in NP cells, we assessed NF-κB pathway activation following TBHP challenge. Our results demonstrated that TBHP treatment significantly upregulated p-p65 expression, increased the p-p65/p65 ratio, and promoted p65 nuclear translocation, indicative of robust NF-κB activation. Strikingly, SIRT7 overexpression substantially attenuated these effects, as evidenced by reduced p65 phosphorylation and impaired nuclear translocation. These results suggest that suppression of NF-κB pathway may contribute to the protective effects of SIRT7 on NP cells.

The needle puncture-induced rat model of IVDD is extensively employed for investigating disease pathogenesis and evaluating therapeutic interventions [28,29], owing to its technical simplicity, reproducibility, and cross-species applicability [30]. We therefore assessed whether SIRT7 overexpression exerts protective effects against IVDD *in vivo*. MRI revealed that needle puncture markedly diminished IVD hydration, whereas SIRT7 overexpression restored water content. Histological evaluation by H&E, Safranin O/Fast Green, and Masson's trichrome staining further confirmed that SIRT7 overexpression attenuated IVDD. Notably, NF-κB signaling was markedly activated in the needle puncture-induced rat IVDD model, an effect that was substantially attenuated by SIRT7 overexpression *in vivo*. Consistently, SIRT7 overexpression downregulated the ECM catabolic marker MMP3, upregulated the anabolic marker collagen II, and reduced Bax expression, indicating its anti-apoptotic and matrix-preserving effects. These results indicate that the inhibition of NF-κB pathway correlates with the protective effects of SIRT7 on NP cells.

This study has several limitations. First, we did not use NF-κB pathway activators or inhibitors to further validate the causal relationship between NF-κB suppression and SIRT7's protective effects. Second, the precise molecular mechanism by which SIRT7 inhibits NF-κB activation, whether through direct p65 deacetylation, IκB kinase (IKK) modulation, or alternative targets, remains to be elucidated. Third, we did not compare SIRT7 with other sirtuin members (e.g., SIRT6) regarding their distinct or overlapping roles in NF-κB inhibition. Addressing these gaps in future studies will strengthen our understanding of SIRT7-mediated protection in IVDD.

5. Conclusions

As far as we are aware, no prior investigation has implicated SIRT7 in the preservation of NP homeostasis. The present study demonstrates that the protective effect of SIRT7 overexpression against IVDD progression correlates with inhibition of the NF-κB signaling pathway both in vitro and in vivo, underscoring its potential as a promising therapeutic target.

Abbreviations

SIRT7, sirtuin 7; IVD, intervertebral disc; IVDD, intervertebral disc degeneration; NP, nucleus pulposus; AF, annulus fibrosus; CEP, cartilaginous endplates; cDNA,

complementary DNA; DHE, dihydroethidium; ECM, extracellular matrix; H&E, hematoxylin and eosin; IHC, immunohistochemistry; Lv-NC, negative control lentivirus; Lv-SIRT7, SIRT7-overexpressing lentivirus; MMP3, matrix metalloproteinase-3; MRI, magnetic resonance imaging; MMP13, matrix metalloproteinase-13; PCR, polymerase chain reaction; qRT-PCR, quantitative reverse transcription polymerase chain reaction; ROS, reactive oxygen species; SD, standard deviation; TBHP, tert-butyl hydroperoxide; $\Delta\Psi m$, mitochondrial membrane potential; NF-κB, nuclear factor kappa B; ANOVA, analysis of variance.

Availability of Data and Materials

The data of this study are available upon reasonable request from corresponding author.

Author Contributions

DW: Conceptualization, Data curation, Investigation, Methodology, Writing original draft. ZY: Data curation, Formal analysis, Methodology, Writing-review & editing. LL: Data curation, Investigation, Writing review & editing. ZC: Data curation, Formal analysis, Writing-original draft. GZ: Data curation, Formal analysis. TL: Data curation, Formal analysis. XK: Con ceptualization, Data curation, Funding acquisition, Methodology, Resources, Supervision, Writing-review & editing. All authors contributed to editorial changes in the manuscript. All authors read and approved the final manuscript. All authors have participated sufficiently in the work and agreed to be accountable for all aspects of the work.

Ethics Approval and Consent to Participate

All the experimental protocols involved in this study were approved by the Ethics Committee of Lanzhou University Second Hospital (2025A-1331). Human-related procedures followed the principles of the Helsinki Declaration, and written informed consent was obtained from every patient before tissue collection. All animal experiments adhered to the ARRIVE guidelines and were reviewed and approved by the Animal Care and Use Committee at Lanzhou University Second Hospital (No. D2025-898).

Acknowledgment

Not applicable.

Funding

This research was funded by the National Natural Science Foundation of China, Grant No.: 82272536, 82560433; the Natural Science Foundation of Gansu province, Grant No.: 25JRRA626; the Cuiying Scientific and Technological Innovation Program of the Second Hospital & Clinical Medical School, Lanzhou University, Grant No.: CY2024-YB-A02; Major Scientific Research Project for Technological Innovation in the Health and Healthcare Sector of Gansu Province, Grant no.: GSWSQNPY2025-02.

Conflicts of Interest

The authors declare no conflicts of interest.

Supplementary Material

Supplementary material associated with this article can be found, in the online version, at https://doi.org/10.31083/FBL50425.

References

[1] Diwan AD, Melrose J. Intervertebral disc degeneration and how it leads to low back pain. JOR Spine. 2023; 6: e1231. https://doi.org/10.1002/jsp2.1231.

[2] Samanta A, Lufkin T, Kraus P. Intervertebral disc degeneration-Current therapeutic options and challenges. Frontiers in Public Health. 2023; 11: 1156749. https://doi.org/10.3389/fpubh.2023.1156749.

[3] Sun H, Guo J, Xiong Z, Zhuang Y, Ning X, Liu M. Targeting nucleus pulposus cell death in the treatment of intervertebral disc degeneration. JOR Spine. 2024; 7: e70011. https://doi.org/10.1002/jsp2.70011.

[4] Xie C, Shi Y, Chen Z, Zhou X, Luo P, Hong C, *et al*. Apigenin Alleviates Intervertebral Disc Degeneration *via* Restoring Autophagy Flux in Nucleus Pulposus Cells. Frontiers in Cell and Developmental Biology. 2022; 9: 787278. https://doi.org/10.3389/fcell.2021.787278.

[5] Zhang Z, Huang Y, Xu N, Wang J, Yao T, Xu Y, *et al*. PLK1 Mitigates Intervertebral Disc Degeneration by Delaying Senescence of Nucleus Pulposus Cells. Frontiers in Cell and Developmental Biology. 2022; 10: 819262. https://doi.org/10.3389/fcell.2022.819262.

[6] Zhang GZ, Liu MQ, Chen HW, Wu ZL, Gao YC, Ma ZJ, *et al*. NF-κB signalling pathways in nucleus pulposus cell function and intervertebral disc degeneration. Cell Proliferation. 2021; 54: e13057. https://doi.org/10.1111/cpr.13057.

[7] Yi W, Chen Q, Liu C, Li K, Tao B, Tian G, *et al*. LIPUS inhibits inflammation and catabolism through the NF-κB pathway in human degenerative nucleus pulposus cells. Journal of Orthopaedic Surgery and Research. 2021; 16: 619. https://doi.org/10.1186/s13018-021-02739-1.

[8] Liang ZH, Song J, Shangguan WJ, Zhang QQ, Shao J, Zhang YH. Melatonin mitigates matrix stiffness-induced intervertebral disk degeneration by inhibiting reactive oxygen species and melatonin receptors mediated PI3K/AKT/NF-κB pathway. American Journal of Physiology. Cell Physiology. 2024; 327: C1236–C1248. https://doi.org/10.1152/ajpcell.00630.2023.

[9] Qiu X, Zhao F, He D, He G, Li X, Liu R, *et al*. BQU57 suppresses IL-1β-induced apoptosis and extracellular matrix degradation in nucleus pulposus cells by blocking the NF-κB signaling pathway. Cellular Signalling. 2025; 131: 111729. https://doi.org/10.1016/j.cellsig.2025.111729.

[10] Kang L, Hu J, Weng Y, Jia J, Zhang Y. Sirtuin 6 prevents matrix degradation through inhibition of the NF-κB pathway in intervertebral disc degeneration. Experimental Cell Research. 2017; 352: 322–332. https://doi.org/10.1016/j.yexcr.2017.02.023.

[11] Raza U, Tang X, Liu Z, Liu, B. SIRT7: the seventh key to unlocking the mystery of aging. Physiological reviews. 2024; 104: 253–280. https://doi.org/10.1152/physrev.00044.2022.

[12] Shen J, Lan Y, Ji Z, Liu H. Sirtuins in intervertebral disc degeneration: current understanding. Molecular Medicine

(Cambridge, Mass.). 2024; 30: 44. https://doi.org/10.1186/s10020-024-00811-0.

[13] Li H, Yuan Z, Wu J, Lu J, Wang Y, Zhang L. Unraveling the multifaceted role of SIRT7 and its therapeutic potential in human diseases. International Journal of Biological Macromolecules. 2024; 279: 135210. https://doi.org/10.1016/j.ijbiomac.2024.135210.

[14] Yamamura S, Izumiya Y, Araki S, Nakamura T, Kimura Y, Hanatani S, *et al*. Cardiomyocyte Sirt (Sirtuin) 7 Ameliorates Stress-Induced Cardiac Hypertrophy by Interacting With and Deacetylating GATA4. Hypertension (Dallas, Tex.: 1979). 2020; 75: 98–108. https://doi.org/10.1161/HYPERTENSIONAHA.119.13357.

[15] Vakhrusheva O, Smolka C, Gajawada P, Kostin S, Boettger T, Kubin T, *et al*. Sirt7 increases stress resistance of cardiomyocytes and prevents apoptosis and inflammatory cardiomyopathy in mice. Circulation Research. 2008; 102: 703–710. https://doi.org/10.1161/CIRCRESAHA.107.164558.

[16] Yu T, Ding C, Peng J, Liang G, Tang Y, Zhao J, *et al*. SIRT7-mediated NRF2 deacetylation promotes antioxidant response and protects against chemodrug-induced liver injury. Cell Death & Disease. 2025; 16: 232. https://doi.org/10.1038/s41419-025-07549-5.

[17] Chen KL, Li L, Li CM, Wang YR, Yang FX, Kuang MQ, *et al*. SIRT7 Regulates Lipopolysaccharide-Induced Inflammatory Injury by Suppressing the NF-*κ*B Signaling Pathway. Oxidative Medicine and Cellular Longevity. 2019; 2019: 3187972. https://doi.org/10.1155/2019/3187972.

[18] Zhang J, Xu C, Tang X, Sun S, Liu S, Yang L, *et al*. Endothelium-specific SIRT7 targeting ameliorates pulmonary hypertension through Krüpple-like factor 4 deacetylation. Cardiovascular Research. 2024; 120: 403–416. https://doi.org/10.1093/cvr/cvae011.

[19] Wu SY, Du YC, Yue CF. Sirt7 protects chondrocytes degeneration in osteoarthritis via autophagy activation. European Review for Medical and Pharmacological Sciences. 2020; 24: 9246–9255. https://doi.org/10.26355/eurrev_202009_23006.

[20] Qiu X, Zhang Y, Wei Z, Luo Z, Wang Z, Kang X. PLGA/BK microspheres targeting the bradykinin signaling pathway as a therapeutic strategy to delay intervertebral disc degeneration. Communications Biology. 2024; 7: 1540. https://doi.org/10.1038/s42003-024-07196-0.

[21] Xie T, Qin W, Zeng D, Wang R, Chen S, Chen Y, *et al*. High-fat diet-induced obesity accelerates puberty in male rats through SMIM20/phoenixin upregulation. Frontiers in Endocrinology. 2025; 16, 1711374. https://doi.org/10.3389/fendo.2025.1711374.

[22] Yang F, Duan Y, Li Y, Zhu D, Wang Z, Luo Z, *et al*. S100A6 Regulates nucleus pulposus cell apoptosis via Wnt/β-catenin signaling pathway: an in vitro and in vivo study. Molecular Medicine (Cambridge, Mass.). 2024; 30: 87. https://doi.org/10.1186/s10020-024-00853-4.

[23] Chen W, Li D, Chen L, Fei J, Bian M, Zeng Q, *et al*. RTA 408 attenuates TBHP-Induced apoptosis in nucleus pulposus cells via Nrf2/ARE and NF-κB signaling pathways: in vitro and in vivo evidence for mitigating rats' intervertebral disc degeneration. Arthritis Research & Therapy. 2025; 27: 128. https://doi.org/10.1186/s13075-025-03588-7.

[24] Chen E, Li M, Liao Z, Yao D, Li Y, Huang L. Phillyrin reduces ROS production to alleviate the progression of intervertebral disc degeneration by inhibiting NF-κB pathway. Journal of Orthopaedic Surgery and Research. 2024; 19: 308. https://doi.org/10.1186/s13018-024-04695-y.

[25] Sun K, Zhu J, Sun J, Sun X, Huan L, Zhang B, *et al*. Neuropeptide Y prevents nucleus pulposus cells from cell apoptosis and IL 1β induced extracellular matrix degradation. Cell Cycle (Georgetown, Tex.). 2021; 20: 960–977. https://doi.org/10.1080/15384101.2021.1911914.

[26] Wang K, Yao D, Li Y, Li M, Zeng W, Liao Z, *et al*. TAK-715 alleviated IL-1β-induced apoptosis and ECM degradation in nucleus pulposus cells and attenuated intervertebral disc degeneration ex vivo and in vivo. Arthritis Research & Therapy. 2023; 25: 45. https://doi.org/10.1186/s13075-023-03028-4.

[27] Wang Y, Cheng H, Wang T, Zhang K, Zhang Y, Kang X. Oxidative stress in intervertebral disc degeneration: Molecular mechanisms, pathogenesis and treatment. Cell Proliferation. 2023; 56: e13448. https://doi.org/10.1111/cpr.13448.

[28] Huo Z, Li D, Zhang K, Yan B, Zhang T, Li Z, *et al*. MGST1 May Regulate the Ferroptosis of the Annulus Fibrosus of Intervertebral Disc: Bioinformatic Integrated Analysis and Validation. Frontiers in Bioscience (Landmark Edition). 2024; 29: 224. https://doi.org/10.31083/j.fbl2906224.

[29] Fu S, Lv R, Wang L, Wang Z, Wang F, Gao H, *et al*. Bone mesenchymal stem cells based on matric hydrogels attenuate intervertebral disc degeneration by suppressing oxidative stress-induced ferroptosis. Scientific Reports. 2025; 15: 15378. https://doi.org/10.1038/s41598-025-00278-x.

[30] Jain C, Huang JJ, Lee Y, Chaudhary S, Hecht AC, Lai A, *et al*. Animal Models of Disc Degeneration Using Puncture Injury: A 20 Year Perspective. JOR Spine. 2025; 8: e70093. https://doi.org/10.1002/jsp2.70093.